JOURNAL OF AIRCRAFT
Vol. 38, No. 3, May–June 2001

Computational Analysis of Centrifugal Compressor Surge Control Using Air Injection

Alexander Stein,* Saeid Niazi,* and Lakshmi N. Sankar†
Georgia Institute of Technology, Atlanta, Georgia 30332-0150

A Navier–Stokes solver for simulating unsteady viscous fluid flow in turbomachinery components has been developed and used to study fluid dynamic phenomena that lead to instabilities in centrifugal compressors. These studies indicate that large flow incidence angles, at reduced flow rates, can cause boundary-layer separation near the blade leading edge. High-pressure jets upstream of the compressor face are studied as a means of controlling compressor instabilities. Steady jets are found to alter the leading-edge flow pattern and effectively suppress compressor instabilities. It is also observed that yawed jets are more effective than parallel jets and that an optimum yaw angle exists for each compression system. Pulsed jets can yield additional performance enhancements and lead to a reduction in external air requirements for operating the jets. Jets pulsed at higher frequencies perform better than low-frequency jets.

Introduction

THE stable operating regime of current generation centrifugal compressors is limited at reduced mass flow rates by two fluid dynamic phenomena: rotating stall and surge. The occurrence of these phenomena defines the surge limit, also referred to as stall line. When operating a compression system under these conditions, strong fluctuations and limit cycle oscillations can cause large vibrations, leading to fatigue and damage of the entire compression unit. Unsteady fluctuations, caused by rotating stall or surge, may lead to excessive heating of the impeller blades and can produce additional periodic loads on the impeller, resulting in increased operating noise levels.

If the fluctuations are left unchecked, even a complete flow reversal is possible, a situation that a compressor cannot tolerate. Because of the severity of these hazardous conditions, centrifugal compressors are conservatively designed to operate well below the peak pressure rise point. A safety margin of 10–20% is generally introduced between the surge line and the design operating condition. Most compressor control systems currently used in industry are based on this strategy, called avoidance control.

Significant progress has been made in the past several years to develop reliable compressor control schemes. These schemes employ fast-response-stall-detection devices, in most cases circumferentially distributed over the casing walls that measure flowfield data and send filtered signals to a controller unit. When a compressor approaches a stall-like condition, the presence of growing instabilities, sometimes called stall precursor waves, is measured and signaled back to the controller unit before the actual stall process begins. The control mechanism is then activated by a direct link between the controller and a set of high-bandwidth actuation devices. The type of control system is often categorized by the choice of a particular actuator.

Pinsley et al.[1] adopted a plenum gate to regulate the flow leaving the compressor. Gysling et al.[2] achieved up to 25% surge margin extension by implementing a movable plenum wall. Arnulfi et al.[3] extended the scheme to a four-stage system. Other types of actuators include high-fidelity plenum loudspeakers,[4] movable inlet guide vanes,[5] synthetic jets,[6] and air injectors upstream of the compressor face.[7–11] The latter scheme was found to be highly effective because most instabilities leading to the development of rotating stall and surge originate near the leading edge. Large leading-edge incidence angles and vortices that form near the blade tip are potential sources of instabilities. Air injection directly energizes regions of low-momentum fluid and reduces the risk of leading-edge separation.

Although much experimental evidence exists proving that air injection is a viable means of alleviating compressor instabilities, it is yet to be determined how the high-pressure jets should be configured and tailored to each individual compressor. Freeman et al.[8] showed that injecting air into the blade tip region of the compressor gives significantly better results than injecting the air into the core of the main compressor flow. Suder et al.[12] illustrated that four half-height valves injecting a total of 0.9% of the main flow rate into the blade tip region yields the same operating enhancements as eight full-height valves using 3.6% of the main flow rate. This reflects a significant reduction in external high-pressure air supply needed. Furthermore, the same authors found that these results were independent of the azimuthal arrangements of these injectors.

Yeung and Murray,[9] Behnken et al.,[10] and D'Andrea et al.[11] reported experimental results of varying injection yaw angles and concluded that the yaw angle is a critical parameter that must be properly tailored to the individual compressor to achieve maximum operating enhancements.

Stein et al.[13] developed a three-dimensional viscous flow solver and studied the fluid dynamic phenomena that lead to the onset of instabilities in a high-speed centrifugal compressor tested at DLR.[14–16] Their results indicated that increased incidence angles trigger leading-edge flow separation, which, in turn, leads to large limit cycle oscillations of the mean flow rate. Time-accurate flow simulations using steady air injection demonstrated the potential of high-pressure jets to alleviate compressor instabilities.

In the present paper, additional computational fluid dynamics (CFD) simulations for the DLR impeller are discussed to gain a better understanding of the stall inception process. The compressor control scheme was extended to include pulsed air injection. Numerical simulations of jets pulsed at different frequencies are analyzed and compared to steady air injection data. Results concerning the optimization of practical air injection systems and implications for future research are also discussed.

Numerical Formulation

In this study, a numerical technique has been employed for simulating fully three-dimensional viscous fluid flow in turbomachinery components. The method solves the unsteady Reynolds-averaged Navier–Stokes equations in integral form and advances the flowfield in a time-accurate manner. The flow equations are solved in a

Received 26 May 2000; revision received 25 July 2000; accepted for publication 8 September 2000.

*Graduate Research Assistant, School of Aerospace Engineering. Student Member AIAA.

†Regents' Professor, School of Aerospace Engineering. Associate Fellow AIAA.

body-fitted rotating coordinate system using an approximate factorization scheme. The inviscid fluxes of mass, momentum, and energy across each of the six faces of a computational cell are computed to third-order accuracy using Roe's approximate Riemann solver.[17] Discretization of the viscous fluxes is performed by using central difference formulations.

A Spalart–Allmaras one-equation model[18] is solved in conjunction with the Navier–Stokes equations to model effects of turbulence.

A detailed description of the numerical formulation of the flow solver including the implicit solution procedure and the boundary conditions is given in Refs. 19 and 20. In these previous studies, the flow solver was also validated against experimental data of a NASA low-speed centrifugal compressor. Niazi et al.[21] further validated the code by applying it to a NASA transonic fan rotor.

Because of limitations in computational resources, a single-flow passage grid is used with blade-to-blade periodic boundary conditions. This approach assumes that the stable operation of centrifugal compressors is limited by instabilities that quickly develop and occur on all flow passages. Instabilities that form and grow across several compressor flow passages in the circumferential direction have been neglected within the framework of this analysis.

Boundary Conditions

No-slip boundary conditions are used at the hub, the casing, and the blade surfaces. The implementation of the inlet boundary condition assumes that the compressor draws air from an upstream reservoir that has a stagnation pressure p_0 and a stagnation temperature T_0. The tangential velocity components at this boundary are set to zero, assuming no swirl inflow, although it is possible within the scope of this study to prescribe swirl or nonuniform stagnation properties at the inlet. At every time step, the speed of sound a and the normal velocity component u_n are determined from a one-dimensional wave equation to account for acoustic and numerical waves leaving the computational domain. Isentropic relations are used to evaluate the inlet density ρ and inlet pressure p.

At the outflow boundary, the foundational assumption is made that the flow from the vaneless diffuser exhausts into a plenum chamber or large reservoir. The coupling between compressor and plenum is essential for the development of compressor instabilities and is accounted for in a phenomenological manner. Assuming negligible fluid velocity and acceleration, spatially uniform pressure and isentropy in the plenum, the pressure is computed from the conservation of plenum mass:

$$\frac{\mathrm{d}p_p}{\mathrm{d}t} = \frac{a_p^2}{V_p}(\dot{m}_c - \dot{m}_t) \tag{1}$$

where $\dot{m}_c$ is the computed mass flow rate at the diffuser plenum interface and $\dot{m}_t$ is the prescribed mass flow rate at the plenum throttle.

Configuration and Grid Generation

The configuration used to investigate instabilities is a high-speed centrifugal compressor (DLRCC) designed and tested at DLR.[14–16] The geometry of this configuration consisting of the impeller and a vaneless diffuser is shown in Fig. 1. It was designed to operate in the high subsonic regime. The corresponding relative Mach numbers range from 0.92 at the rotor inlet to 0.96 at the rotor exit. These values were measured at a design rotational shaft speed of 22,360 rpm, at a mass flow rate of 4.0 kg/s and a pressure ratio of 4.7. The DLRCC was designed by a CAD/CAM procedure developed at DLR,[22] and the impeller was manufactured on a five-axis milling machine. Therefore, the blade surfaces were generated by straight lines that run from hub to tip.

The computational H mesh used to simulate flow in the DLRCC is also shown in Fig. 1. The single flow passage grid has the dimensions $141 \times 49 \times 33$ in the streamwise, spanwise, and pitchwise directions, respectively. Eight layers of computational cells are placed in the clearance gap.

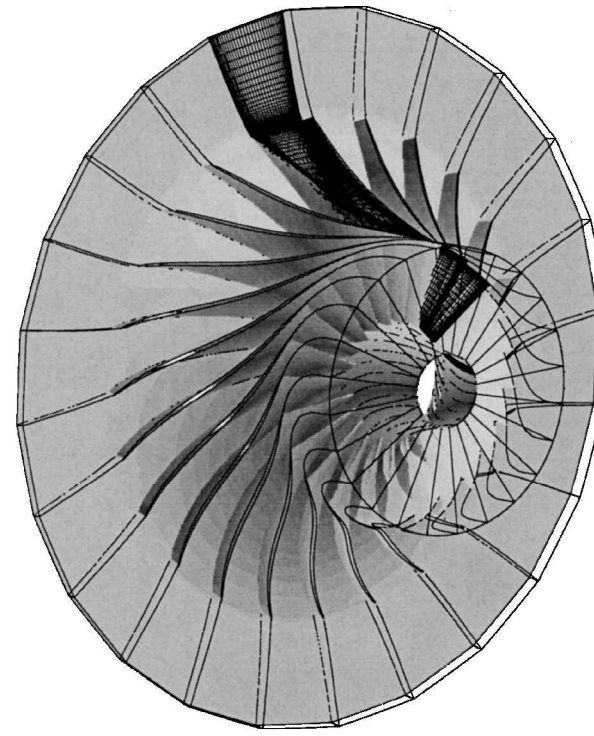

Fig. 1 Single flow passage computational grid for DLR high-speed compressor with dimensions $141 \times 49 \times 33$ in the streamwise, spanwise, and pitchwise directions.

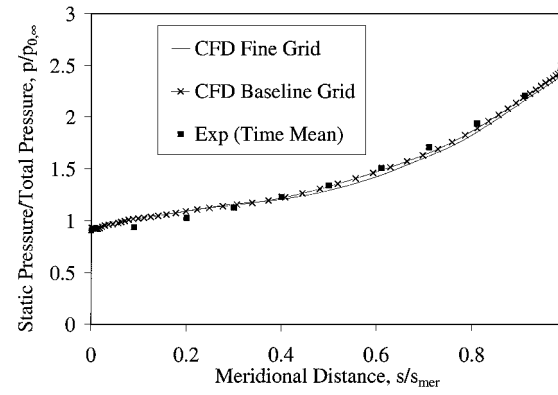

Fig. 2 Circumferentially averaged static pressure along shroud, $p/p_{0\infty}$, operating design conditions (4.0 kg/s).

Results and Discussion

All numerical simulations were computed on a high-performance Silicon Graphics Origin 2000 with multiple processors, using either four or six processors per run. To resolve the dominant length scales of compressor instabilities, small computational time steps were chosen. For all of the calculations, the computational time step was set to yield approximately one degree of rotor revolution per 25 time steps. With this time step, the flowfield simulation of one rotor revolution required about 9000 computational steps, consuming approximately 5–6 h of elapsed wall clock time on the Origin 2000 using four processors. Because a large number of unsteady runs were required during this study, the maximum number of processors was restricted to six. The additional processors available on the computer were used to execute multiple runs simultaneously.

Validation Results and Grid Sensitivity Study

A limited number of calculations at design conditions (4.0-kg/s mass flow rate) were done to validate the flow solver and the grid against experimental data. The predicted pressure ratio at this operating point was 4.5. This computed value underpredicted the measured result ($\pi = 4.7$) by approximately 4%. Figure 2 shows the results

of a grid sensitivity study and a comparison between experimental and computational data. The experimental shroud pressures were measured at several locations along the shroud meridional chord and were then time averaged over the duration of the measurement cycle. The CFD calculations were performed using two different computational grids. The results labeled CFD baseline grid were produced with the mesh plotted in Fig. 1. To demonstrate grid insensitivity of these results, a second grid with twice the number of grid points in each direction was tested. The dimensions of the grid labeled CFD fine grid in Fig. 2 were $281 \times 97 \times 65$. The computed static shroud pressures from this analysis, however, showed nearly the same result regardless of the grid used. Consequently, the baseline grid was assumed to be sufficient for capturing the main flow phenomena in the DLRCC with reasonable accuracy. Because of limitations in computational resources, this grid was utilized in all subsequent discussions. These results have been presented in a previous study,[13] but are included here to provide a baseline for the following studies.

Off-Design Results

Figure 3 shows a comparison between the calculated and the experimental DLRCC performance map. In an attempt to quantify the flow unsteadiness at each computed operating point, circles are added to the time-averaged mean flow data where the size of each circle indicates the magnitude of the flow rate and pressure rise fluctuations. The graph depicts the large increase in limit cycle oscillations at reduced flow rates.

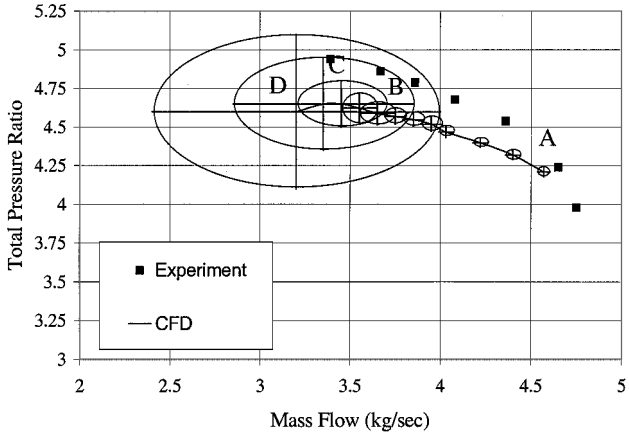

Fig. 3a DLRCC performance map with the amplitude of the fluctuations denoted by circles.

In addition to the performance map data, Fig. 3 shows the time history for four selected points, A–D, on the performance map. The four points chosen were A, mass flow rate of 4.6 kg/s (stable operation); B, mass flow rate of 3.75 kg/s (stable operation with increased fluctuations); C, mass flow rate of 3.4 kg/s (peak pressure point, onset of stall); and D, mass flow rate of 3.2 kg/s (unstable operation).

Plots A–D show the fluctuations in mass flow rate and pressure ratio at each selected operating condition. At the stable operating point, A, referred to as an attractor, fluctuations in mass flow rate and pressure rise were less than 1%. As the mass flow rate was decreased, the fluctuations increased to 2–3% (point B) and 10% (point C) near the point of maximum pressure rise. A further reduction in mass flow caused the performance map to drop off, which was again accompanied by a large increase in fluctuations, namely, 20–30% at point D. In this case, much of the flow through the impeller was stalled.

Figure 4 depicts the fluid dynamic phenomena that contributed to the development of the large limit cycle oscillations at point D just described. These flowfield snapshots, taken at the midpassage near the leading edge at various time levels over the period of one limit cycle, T_{stall}, reveal the growth of a large separation zone. This separation zone originates at the tip of the impeller leading edge (at $t = 0.25T_{\text{stall}}$) as a result of increased incidence angles and extends downstream into the compressor. At $t = 0.5T_{\text{stall}}$, approximately 25% of the leading-edge span is stalled. Because this reversed flow region is located near the compressor casing, it may be concluded that the vortex flow pattern that forms in compressors as a result of tip clearance leakage also contributed to this instability. The reversed flow caused the downstream plenum pressure to drop, which allowed the flow to gradually recover (at $t = 0.75T_{\text{stall}}$) and the blade boundary layer to reattach. The limit cycle was then repeated.

Steady Air Injection Control

In this study, both steady and unsteady air injection upstream of the compressor face were tested as open-loop compressor control schemes. Figure 5 shows a schematic of the injectors used in this

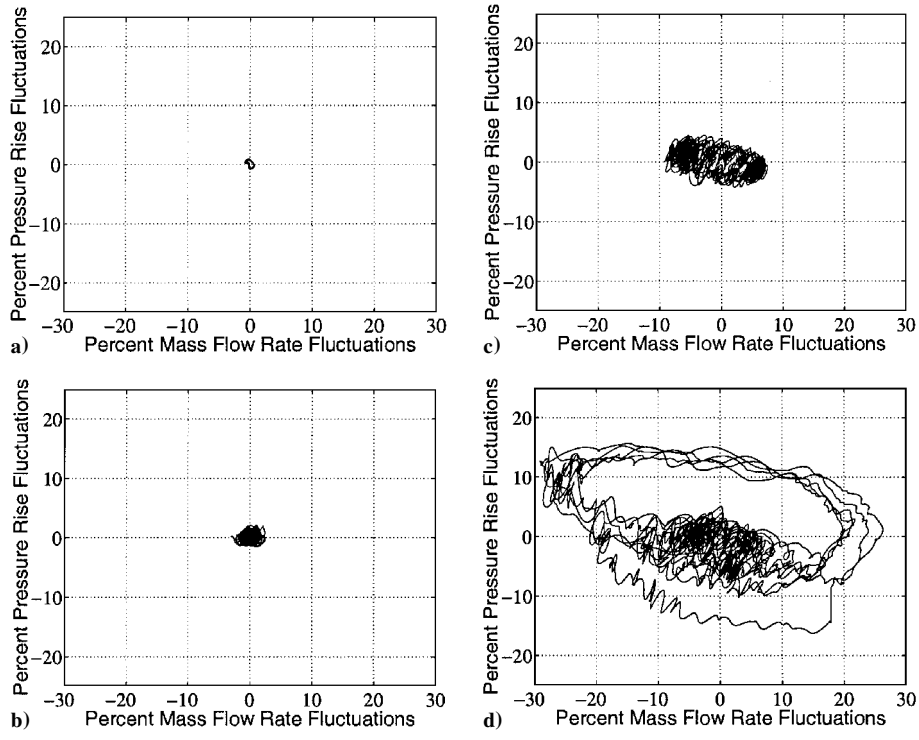

Fig. 3b Time history for selected points A–D of performance map.

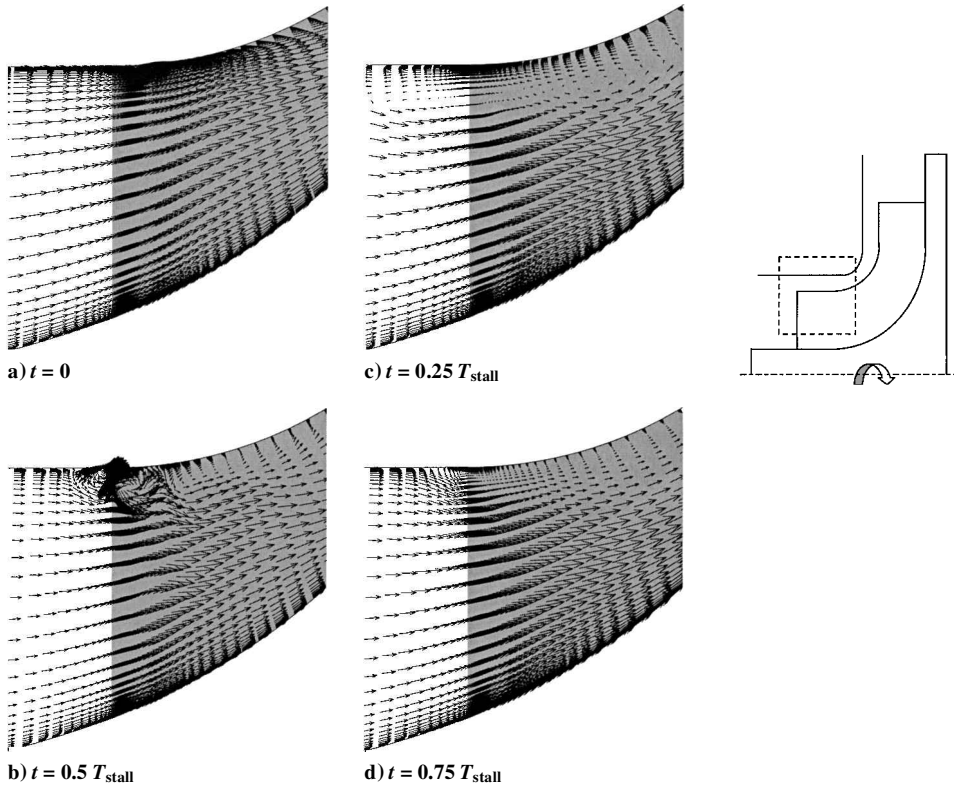

Fig. 4 Velocity vectors near leading edge during limit cycles at midpassage; shading indicates the impeller region.

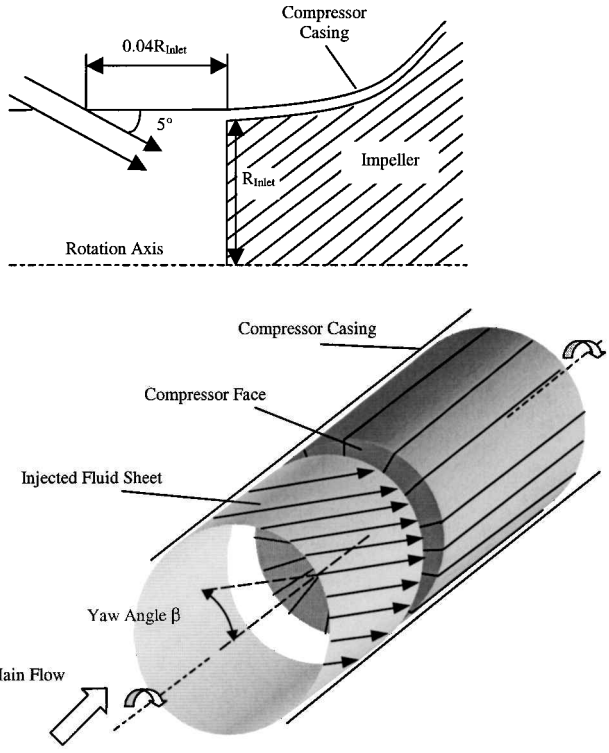

Fig. 5 Schematics of air injection setup and injected fluid sheet.

study. It was assumed that a ring injector continually blows air into the tip region of the rotor to alter and energize the leading-edge flow, which in turn suppresses vortex shedding or boundary-layer separation. The ring injector is formed by a small opening azimuthally encircling the entire compressor annulus. This method requires a significant amount of external high-pressure air. Experiments[12] have shown that by using only four sheet injectors, the same effect of stabilizing the compressor may be achieved as with a greater number of injectors or with the ring injector employed in this study. Thus, the requirements for effective stall control may be much smaller than outlined in this study, which could make air injection control even more desirable to engine designers.

The ring injectors were placed a short distance, 10% of the inlet tip radius, upstream of the compressor face. The objective of this was to achieve maximum control over the leading-edge flow by varying individual injection parameters. A limited number of preliminary computations with twice the amount of spacing between the injectors and the compressor face revealed no significant changes in the control effectiveness of the jets.

The injection angle α was set to 5 deg, whereas the yaw angle β, schematically shown in Fig. 5, was parametrically varied. The injection angle was conservatively chosen with the intention of generating a high-momentum fluid sheet to prevent the growth of the leading-edge separation near the blade tip. Parametric studies were subsequently performed with varying yaw angles and with varying injection rates to find the optimum injection configuration that gives maximum operating enhancements with the least amount of external air supply. Figure 6 shows the results of this parametric study in three-dimensional graphs. The nondimensional surge amplitude on the vertical axis is defined as the ratio of the mass flow rate fluctuations with injection control and the computed mass flow rate fluctuations without injection control. In this analysis, positive yaw angles were measured relative to the compressor face in a direction opposite to the blade rotational motion.

A total of 30 unsteady CFD simulations with 5 injection rates and 6 yaw angles were performed. The computed data for the high-speed compressor illustrate that there is an optimum injection configuration for which the mass flow fluctuations are decreased to 14.7% of the predicted computed mass flow amplitude without injection control. This operating condition corresponds to a yaw angle setting between 5 and 10 deg and an injection rate of 3.2%. Clearly, for departures from the optimum configuration in both yaw angle and injection rate, the fluctuations grow and the compressor operation becomes less effective. The growing surge amplitude for higher injection rates can be explained by the increased ratio of jet velocities to mean flow velocities. In this case, little momentum transfer took place between injected fluid particles and fluid particles of low

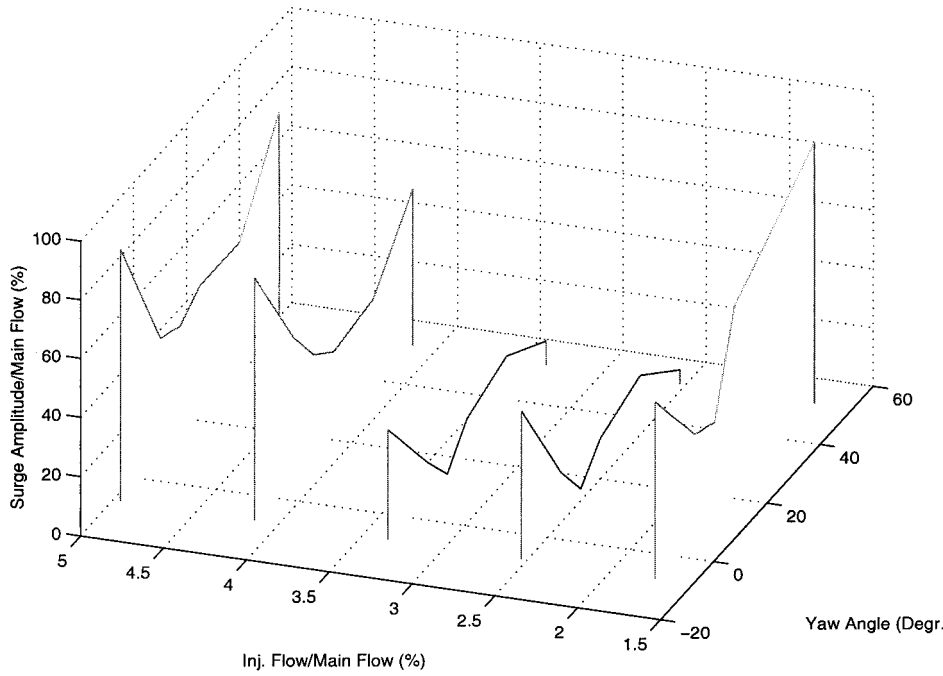

Fig. 6 Parametric study with different yaw angles and different injection rates.

momentum near the leading-edge boundary layer. As a result, higher injection ratios were less efficient and should be avoided for best results.

Pulsed Air Injection Control

Experiments[7] have shown that additional performance enhancements can be obtained by going from steady to pulsed air injection. The first advantage of pulsed air injection is the significant reduction in external air supply requirements while retaining the same favorable flow control characteristics. Second, a thorough knowledge of the system dynamics and a careful choice of the actuation properties amplitude, frequency, and phase angle proved to cancel out effectively unstable modes and suppress compressor instabilities. The type of pulsed air injection used in this study was of the form

$$\dot{m}_{\text{inj}}(t)/\bar{\dot{m}}_{\text{flow}} = I_{\text{inj}} + A_{\text{inj}} \sin(\omega_{\text{inj}} t) \tag{2}$$

where $\dot{m}_{\text{inj}}$ is the injected mass flow rate, I_{inj} and A_{inj} are percent fractions of the time-averaged mass flow rate through the compressor, and ω_{inj} is the user-specified injection frequency. A mean injection rate of 1.5% was computationally tested by CFD methods. The optimum DLRCC yaw angle found from steady injection ($\beta = 7.5$ deg) was used for the pulsed injection. The remaining parameters in the pulsed injection setup, injection angle, injector spacing, injector arrangement, and injection area were the same as in the steady injection.

Figure 7 shows the nondimensional mass flow rate fluctuations and the local incidence angle variations as a function of time at a mean mass flow rate of 3.2 kg/s and an injection rate of $0.015 + 0.015 \sin(\omega_{\text{stall}} t)$. The injection frequency was set equal to the first harmonic frequency of the limit cycle oscillations, ω_{stall}, determined from time-accurate CFD simulations without compressor control. The graph reveals that the compressor instabilities decreased by a factor of five as long as the injection phase angle was lagged 180 deg behind the flow phase angle. Because of small shifts in the first harmonic frequency during injection, the injection phase angle had to be adjusted several times during the calculations to remain exactly 180 deg behind the flow phase angle. After approximately 13 rotor revolutions, the injection rate was left frozen, thus causing the incidence angles to increase to almost 100 deg and the fluctuations in mass flow rate to reach values that were predicted during limit cycle oscillations without injection control.

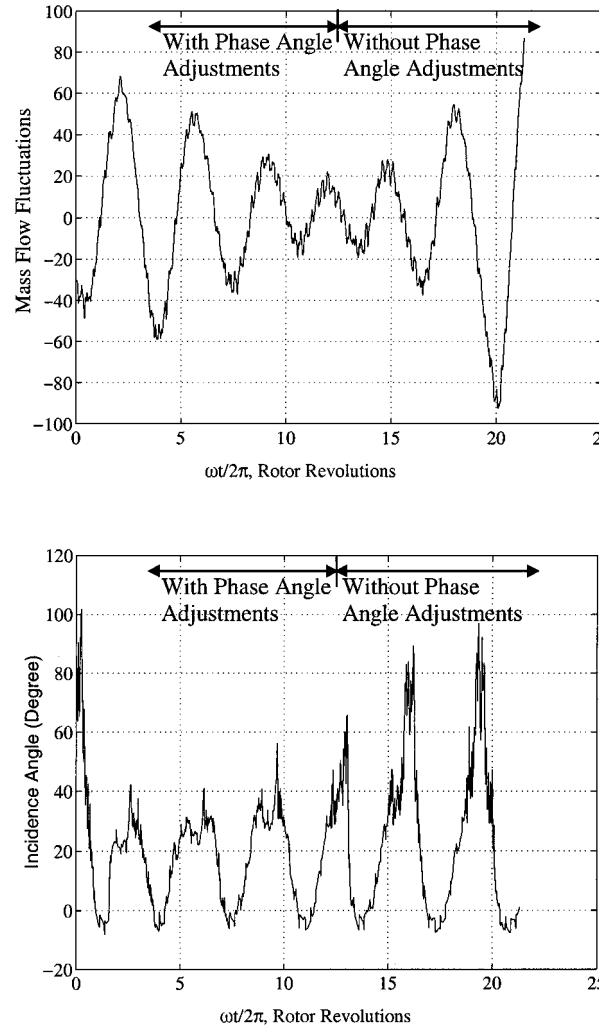

Fig. 7 Mass flow rate fluctuations and incidence angles at 3.2 kg/s mean mass flow rate, 7.5 deg yaw angle, and 0.015 + 0.015 sin($\omega_{\text{stall}} t$) pulsed injection rate.

This observation reemphasizes the importance of phase angle adjustments, a technique that can be automated in feedback compressor controllers. Feedback control schemes measure the growth of stall-precursor signals at a limited number of compressor locations.[23] This information is then sent to a controller unit that in turn regulates the mean, the amplitude, and the phase angle of the pulsed injection.

Figure 8 shows a series of velocity vector snapshots at midpassage and at different instances in time over the period of one limit cycle, T_{stall}. The label $t = 0$ refers to the instance when the flow rate reached a maximum and the label $t = 0.5T_{\text{stall}}$ denotes the instance of minimum flow rate. The corresponding injection signal was lagged 180 deg behind the flow phase angle throughout the entire cycle. To illustrate the effectiveness of the applied compressor control, pulsed air injection of the form $0.015 + 0.015 \sin(\omega_{\text{stall}} t)$ was applied to the DLRCC at the location depicted in Fig. 8a. Vertical lines in each respective snapshot indicate the positions of the blade leading edges. Figure 8a shows the flowfield at the instantaneous point of maximum flow rate. At this point, the boundary layers remained attached even though no air was injected. After 25% of the cycle (Fig. 8b), a small separation region developed near the tip leading edge because the instantaneous injection rate (0.4%) at this point was not strong enough to energize the fluid particles. Figures 8c–8e show the flowfield at minimum flow rate. Figures 8c–8e illustrate how the injected air mixed with low-momentum fluid in the tip recirculation regions, thus causing the stalled flow to recover. The instantaneous injection rate corresponding to Figs. 8c–8e was approximately 3%. The situation shown in Fig. 8f indicates that after 75% of the cycle the entire recirculation region has vanished and the process is repeated.

Figure 9 illustrates how the injection frequency ω_{inj} should be specified to optimize pulsed injection. These calculations were performed with an injection frequency of $4\omega_{\text{stall}}$. The results from this study show that jets pulsed at higher harmonics of the stall frequency reduce the surge fluctuations well below 10%, despite predicted incidence angles between 50 and 60 deg. These data suggest that a short, temporary boost from the injection valves is sufficient to stabilize the flow and suppress instabilities. Consequently, higher injection frequencies should be utilized for best performance.

Additional CFD simulations with injection frequencies above $\omega_{\text{inj}} = 4\omega_{\text{stall}}$ were not attempted; however, further improvements in stall alleviation can be expected for these calculations. This was

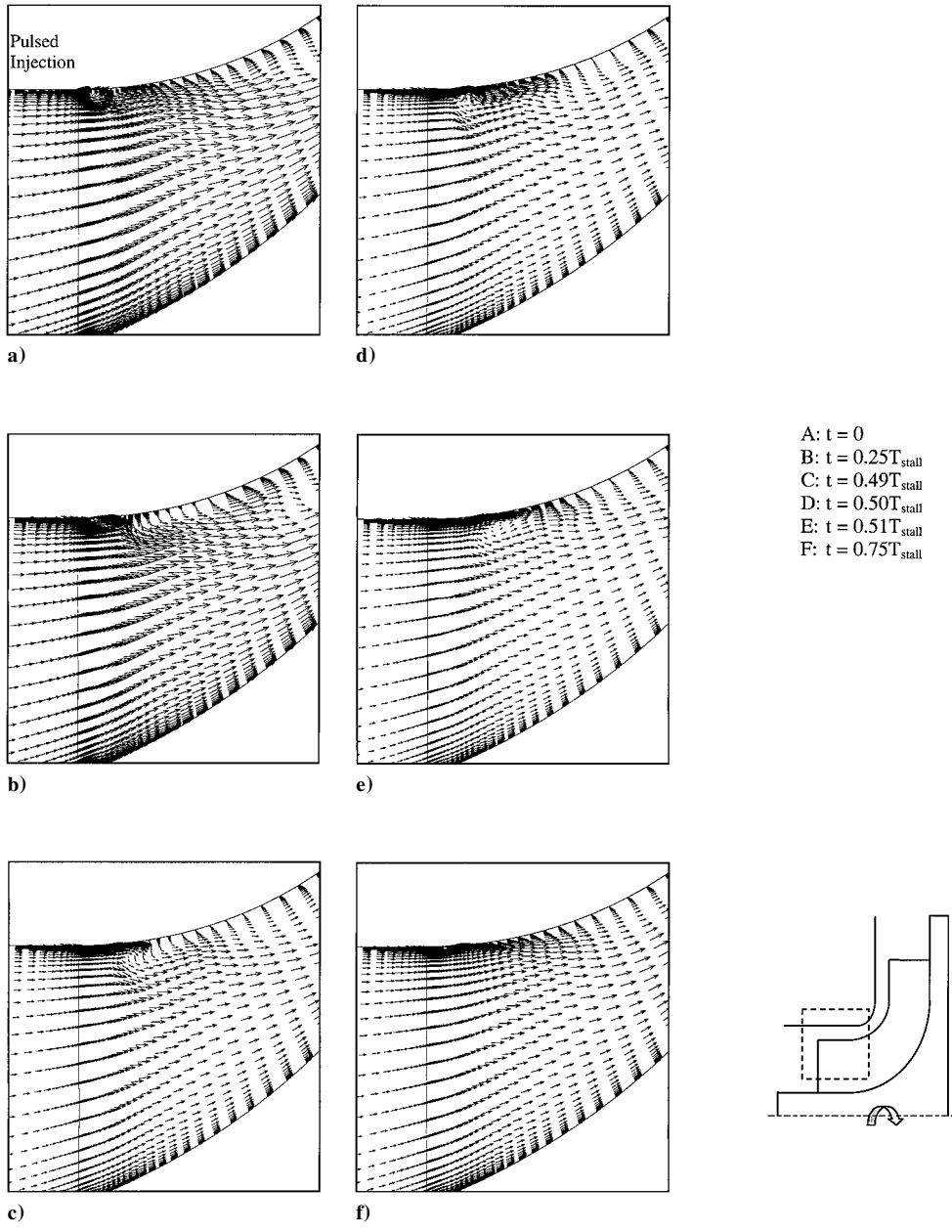

Fig. 8 Velocity vector snapshots at midpassage at 3.2 kg/s mean mass flow rate, 7.5 deg yaw angle, and $0.015 + 0.015 \sin(\omega_{\text{stall}} t)$ pulsed injection rate.

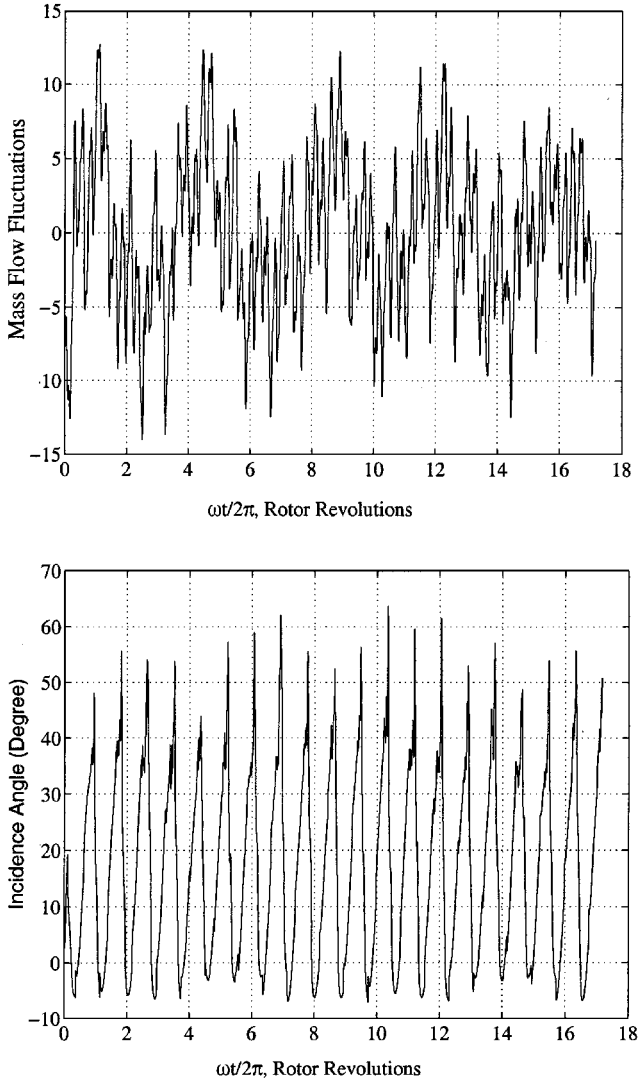

Fig. 9 Mass flow fluctuations and incidence angles at 3.2 kg/s mean mass flow rate, 7.5 deg yaw angle, and 0.015 + 0.015 sin($4\omega_{stall}t$) pulsed injection rate.

done with the impetus that real compressor actuators are limited in bandwidth; therefore, compressor designers prefer actuation systems that provide stability and robustness at low frequencies.

In an attempt to understand the underlying fluid dynamic phenomena that lead to effective air injection control in centrifugal compressors, the flowfield near the leading-edge blade tip was investigated using no jets, low-frequency jets($\omega_{inj} = \omega_{stall}$), and high-frequency jets ($\omega_{inj} = 4\omega_{stall}$). Figure 10 shows a comparison of vorticity magnitudes at a fixed location downstream of the leading edge for the three cases considered. These data were collected over the duration of approximately four rotor revolutions at midpassage and 99% span. The streamwise location of the probe was $0.025R_{inlet}$ downstream of the leading edge. Figure 10 illustrates that the vorticity magnitudes without forcing are significantly lower than the computed vorticity with forcing. When there is no forcing, the vorticity peaks at only two points: after approximately one rotor revolution and after four rotor revolutions. These peaks correspond to Figs. 4b and 4d, which depict local flow separation and recovery at the probe location.

The time-averaged vorticity magnitudes with jet control are almost 250% of the mean magnitudes in the unforced case. This indicates that during most of the sample period increased amounts of mixing enhance the momentum transfer from the injected fluid to the low-kinetic energy particles in the separation zone.

Figure 11 gives additional insight into the fluid dynamic phenomena that lead to a better performance of jets pulsed at higher frequencies than low-frequency jets. Figure 11 shows a comparison of shear stresses caused by jets pulsed at $\omega_{inj} = \omega_{stall}$ and jets pulsed at $\omega_{inj} = 4\omega_{stall}$. The CFD data was ensemble averaged over the region indicated in the schematic. This region extends from the leading edge to approximately $0.3R_{inlet}$ downstream, from 85% span to the compressor casing and across the entire azimuthal direction of the flow passage. The results indicate that high-frequency actuation leads to significantly larger shear stress levels compared to low-frequency actuation. When time-averaged over the entire sample period, this increase rises as high as 30%. Shear stress peaks at high-frequency forcing are almost twice as large as the maximum stresses observed at low-frequency pulsing. Additional investigations reveal that shear stresses in the core of the high-frequency jet are 75% larger than for the low-frequency jet.

These findings suggest that increased fluid dynamic stresses at high-level excitation produce smaller but intense turbulent eddies. This mechanism enhances the mixing of small length scales, thus improving the transfer of momentum and energy from the jet to the

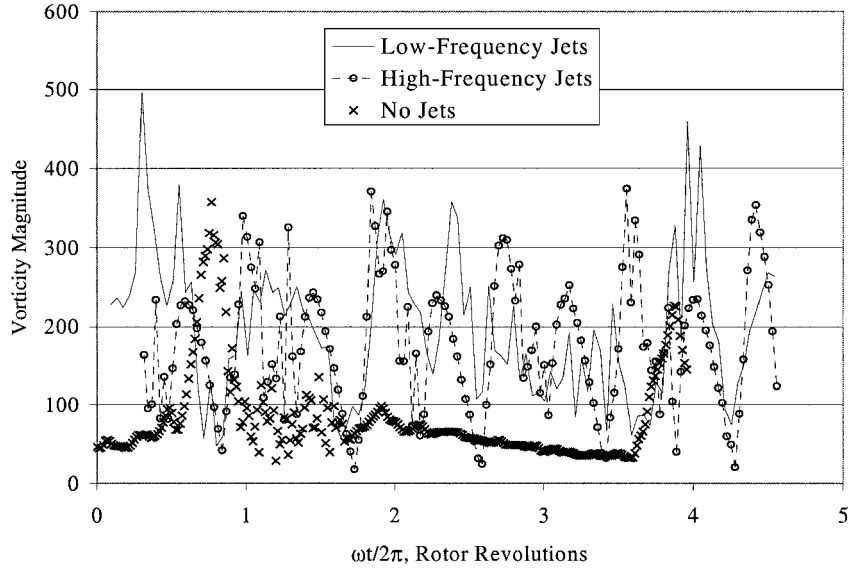

Fig. 10 Comparison of vorticity magnitudes using no jets, low-frequency jets ($\omega_{inj} = \omega_{stall}$), and high-frequency jets ($\omega_{inj} = 4\omega_{stall}$); data were collected at midpassage, 99% span, and $0.025R_{inlet}$.

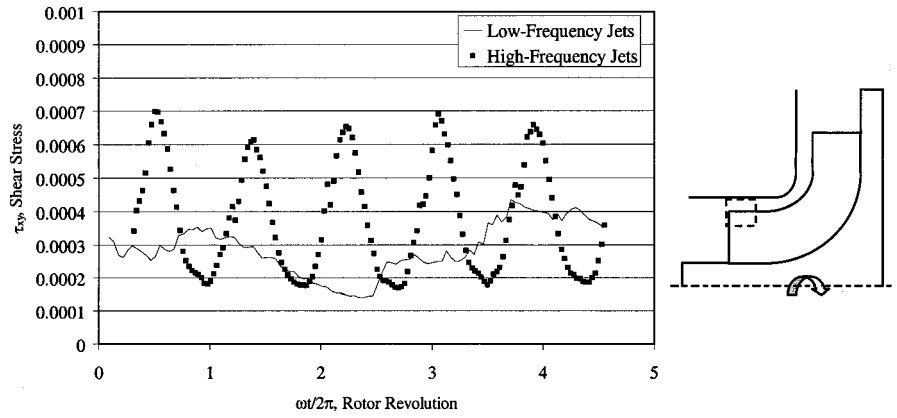

Fig. 11 Comparison of shear stresses τ_{xy} using low-frequency jets ($\omega_{inj} = \omega_{stall}$) and high-frequency jets ($\omega_{inj} = 4\omega_{stall}$); data were ensemble-averaged over the region indicated in the schematic.

low-momentum fluid. As a result, the separation region vanishes and the onset of compressor instabilities is suppressed.

Concluding Remarks

A numerical technique has been developed for simulating fully three-dimensional viscous fluid flow in turbomachinery components. This time-accurate method has been applied to study blade tip flow separation leading to instabilities in centrifugal compressors. Steady jets are found to be effective in controlling these instabilities. They alter the local incidence angles and suppress boundary-layer separation. Because an optimum yaw angle exists for each configuration, yawed jets perform better than parallel jets. Pulsed jets are more effective than steady jets for suppressing instabilities. Jets pulsed at higher harmonics of the stall frequency produce larger shear stresses than low-frequency jets and better energize the injected particles. However, due to saturation, there is a practical limitation on the highest possible frequency.

Acknowledgments

The authors were supported by the U.S. Army Research Office under the Multidisciplinary University Research Initiative on Intelligent Turbine Engines. David Mann was the Technical Monitor. High-performance computer time was provided by the Major Shared Resource Center of the U.S. Army Engineer Research and Development Center. The authors are thankful to Stephen Davis for providing this computer time.

References

[1]Pinsley, J. E., Guenette, G. R., Epstein, A. H., and Greitzer, E. M., "Active Stabilization of Centrifugal Compressor Surge," *Journal of Turbomachinery*, Vol. 113, No. 4, 1990, pp. 723–732.

[2]Gysling, D. L., Dugundji, J., Greitzer, E. M., and Epstein, A. H., "Dynamic Control of Centrifugal Compressor Surge Using Tailored Structures," American Society of Mechanical Engineers Paper 90-GT-122, June 1990.

[3]Arnulfi, G. L., Giamattasio, P., Massado, A. F., Micheli, D., and Pinamonti, P., "Multistage Centrifugal Compressor Surge Analysis: Part II—Numerical Simulation and Dynamic Control Parameters Evaluation," *Journal of Turbomachinery*, Vol. 121, No. 1, 1999, pp. 312–320.

[4]Ffowcs Williams, J. E., and Huang, X. Y., "Active Stabilization of Compressor Surge," *Journal of Fluid Mechanics*, Vol. 204, July 1989, pp. 245–262.

[5]Paduano, J. D., Epstein, A. H., Valvani, L., Langley, J. P., Greitzer, E. M., and Guenette, G. R., "Active Control of Rotating Stall in a Low-Speed Axial Compressor," *Journal of Turbomachinery*, Vol. 115, No. 1, 1993, pp. 48–56.

[6]Breuer, K., Schmidt, M., and Epstein, A. H., "Active Control of Air-Breathing Propulsion Using MEMS," Massachusetts Inst. of Technology Year-End Rept., Dept. of Aerospace Engineering, Cambridge, MA, July 1998.

[7]Lawless, P. B., and Fleeter, S., "Active Control of Rotating Stall in a Low-Speed Centrifugal Compressor," *Journal of Propulsion and Power*, Vol. 15, No. 1, 1999, pp. 38–44.

[8]Freeman, C., Wilson, A. G., Day, I. J., and Swinbanks, M. A., "Experiments in Active Control of Stall on an Aeroengine Gas Turbine," American Society of Mechanical Engineers Paper 97-GT-280, June 1997.

[9]Yeung, S., and Murray, R. M., "Reduction of Bleed Valve Requirements for Control of Rotating Stall Using Continuous Air Injection," *Proceedings of the 1997 IEEE International Conference on Control Applications*, IEEE Publications, Piscataway, NJ, 1997, pp. 683–690.

[10]Behnken, R. L., Leung, H., and Murray, R. M., "Characterizing the Effects of Air Injection on Compressor Performance for use in Active Control of Rotating Stall," American Society of Mechanical Engineers Paper 97-GT-316, June 1997.

[11]D'Andrea, R., Behnken, R. L., and Murray, R. M., "Rotating Stall Control of an Axial Flow Compressor Using Pulsed Air Injection," *Journal of Turbomachinery*, Vol. 119, No. 4, 1997, pp. 742–752.

[12]Suder, K. L., Thorp, S. A., Starzisar, A. J., and Bright, M. M., "Compressor Stability Enhancement Using Discrete Tip Injection," American Society of Mechanical Engineers Paper 2000-GT-0650, May 2000.

[13]Stein, A., Niazi, S., and Sankar, L. N., "Numerical Analysis of Stall and Surge in a High-Speed Centrifugal Compressor," AIAA Paper 2000-0226, Jan. 2000.

[14]Krain, H., and Hoffmann, W., "Centrifugal Impeller Geometry and Its Influence on Secondary Flows," CP-469, AGARD, 1990, pp. 12.1–12.17.

[15]Krain, H., and Hoffmann, W., "Verification of an Impeller Design by Laser Measurements and 3D-Viscous Flow Calculations," American Society of Mechanical Engineers Paper 89-GT-159, June 1989.

[16]Krain, H., "Swirling Impeller Flow," *Journal of Turbomachinery*, Vol. 110, No. 1, 1988, pp. 122–128.

[17]Roe, P. L., "Approximate Riemann Solvers, Parameter Vectors, and Difference Schemes," *Journal of Computational Physics*, Vol. 135, No. 2, 1997, pp. 250–258.

[18]Spalart, P. R., and Allmaras, S. R., "A One-Equation Turbulence Model for Aerodynamic Flows," AIAA Paper 92-0439, Jan. 1992.

[19]Niazi, S., Stein, A., and Sankar, L. N., "Development and Application of a CFD Solver to the Simulation of Centrifugal Compressors," AIAA Paper 98-0934, Jan. 1998.

[20]Stein, A., Niazi, S., and Sankar, L. N., "Computational Analysis of Stall and Separation Control in Centrifugal Compressors," AIAA Paper 98-3296, July 1998.

[21]Niazi, S., Stein, A., and Sankar, L. N., "Numerical Studies of Stall and Surge Alleviation in a High-Speed Transonic Fan Rotor," AIAA Paper 2000-0225, Jan. 2000.

[22]Krain, H., "A CAD-Method for Centrifugal Impellers," *Journal of Engineering for Power*, Vol. 106, No. 3, 1984, pp. 482–488.

[23]Prasad, J. V. R., Neumeier, Y., and Krichene, A., "Active Control of Compressor Surge Using a Real Time Observer," *Proceedings of the NATO Symposium on Active Control Technology for Enhanced Performance Operational Capabilities of Military Aircraft, Land Vehicles and Sea Vehicles*, Braunschweig, Germany, May 2000.